Soft Matter

Emergence of an Apparent Yield Phenomenon in the Mechanics of Stochastic Networks with Inter-Fiber Cohesion

Journal:	*Soft Matter*
Manuscript ID	SM-ART-10-2023-001315.R1
Article Type:	Paper
Date Submitted by the Author:	16-Nov-2023
Complete List of Authors:	Amjad, Syed Nabeel; Rensselaer Polytechnic Institute, Department of Mechanical, Aerospace and Nuclear Engineering Picu, Catalin; Rensselaer Polytechnic Institute,

Emergence of an Apparent Yield Phenomenon in the Mechanics of Stochastic Networks with Inter-Fiber Cohesion

S.N. Amjad and R.C. Picu[1]

Department of Mechanical, Aerospace and Nuclear Engineering, Rensselaer Polytechnic Institute, Troy, NY 12180

Abstract

In this work we investigate the contribution of inter-fiber cohesion to defining the mechanical behavior of stochastic crosslinked fiber networks. Fibers are athermal and store energy primarily in their bending and axial deformation modes. Cohesion between fibers is defined by an interaction potential. These structures are in equilibrium with the inter-fiber cohesive forces before external load is applied and their mechanical behavior is probed in uniaxial tension. Two types of configurations are considered: a state with high initial free volume in which contacts between fibers are scarce, and a state with low free volume and large number of fiber contacts. While in the absence of cohesion the response is hyperelastic, we observe that a yield point-like phenomenon develops as the strength of cohesion increases in both network types considered; we refer to this as an 'unlocking phenomenon'. The small strain stiffness increases as cohesion becomes more pronounced. The stiffness and unlocking stress are expressed in terms of network parameters and cohesion strength through a product of two functions, one dependent on network parameters only, and the other is a function of the cohesion strength. While the small strain response is controlled by cohesion, the large strain behavior is shown to be largely controlled by the network. Therefore, varying the strength of cohesion has no effect on strain stiffening. These observations provide a physical basis for the unlocking observed in both athermal and thermal network materials and are expected to facilitate the design of soft materials with novel properties.

Keywords: network materials; cohesion; adhesion; mechanical behavior.

[1] Corresponding author: Tel: 1 518 276 2195; e-mail: picuc@rpi.edu.

1. Introduction

The broad class of network materials includes materials whose mechanical behavior is controlled by an underlying network of fibers[1]. Examples are abundant: the extracellular matrix[2], the dermis[3], various collagen-based membranes within the human/animal body[4,5] are biological network materials, while paper and nanopapers[6,7], nonwovens and textiles[8,9] are examples of man-made network materials. In all these cases, fibers are randomly oriented, and the network is stochastic. Further, fibers forming these materials are large enough for thermal fluctuations to be irrelevant for their mechanics and hence are athermal. Thermal networks, which include gels, elastomers, and entangled thermoplastics, form a distinct class of network materials.

The interactions of fibers within the network are of bonded and non-bonded type. Bonded interactions include those taking place at crosslinks. In athermal networks, where fibers store energy primarily in the bending and axial modes, the crosslinks transmit both forces and moments. Non-bonded interactions take place at contacts. In a dense network in which many contacts are established, not all contacts transmit load, and some may open and reform elsewhere during deformation. Cohesive interactions are also of non-bonded type and may be caused by hydrogen bonding, hydrophobic interactions, electrostatic interactions, etc[10]. Such energetic interactions as well as entropic interactions tend to align fibers and cause bundling[11], leading to an isotropic to nematic transition[12]. In general, since cohesion forces are short-ranged, fibers of diameter in the micron range and larger must be brought into proximity by other means for cohesion to be effective. Capillarity causes various effects in soft materials composed from athermal fibers and may induce large deformations, stiffening, and preferential fiber alignment[13]. Nonwovens may be 'mechanically activated' – a procedure which aligns fibers and increases the stiffness and strength in the direction of alignment[14]. If fibers are not crosslinked, such as in the case of suspensions, cohesion leads to bundling[15,16]. Carbon nanotubes that grow in a furnace in the presence of carbonaceous species and catalysts develop strong adhesive forces as they come in contact and form bundles that sediment to form buckypaper[17]. Nanoscale filaments, including individual molecules, develop strong adhesive forces. Such interactions provide the cohesive strength of polymeric melts and produce the glass transition as temperature is reduced. This brief overview indicates that cohesive forces may become the dominant type of interactions in certain network materials.

Network materials are studied by various communities in connection with diverse applications. The mechanical behavior of various athermal material systems is described in Ref. 1. Fibers typically represent only a few percent of the total volume of the material, which mandates that contact formation is a rare event in tension and shear; however, it becomes essential in compression[18]. In the absence of cohesive interactions and inter-fiber contacts, the behavior is controlled by the network structure and fiber properties[1,19–21]. Dense networks (the density, ρ, is defined as the total length of fiber per unit volume) of relatively thick fibers (d is the fiber diameter), deform affinely, i.e. the strain experienced by individual fibers is identical to the macroscopic applied strain. In this case, the small strain network stiffness, E_0, is $E_0 \sim \rho d^2$. In most practical cases networks are sparse and/or are made of fibers of large aspect ratio. In such situations, deformation is non-affine, and $E_0 \sim \rho^x d^4$, with x being a function of the network

architecture. In 3D, $x = 2$ for cellular networks such as Voronoi, $x = 3$ for fibrous networks and takes larger values in 2D[22]. The affine-non-affine transition is controlled by the non-dimensional parameter $w = \log_{10}\rho d^2$, with low w values corresponding to non-affine behavior. Networks of this type exhibit hyperelastic behavior under large deformation, characterized by exponential stiffening[1,23–25].

Networks with lower free volume, in which non-bonded interactions become important, exhibit a somewhat different behavior, with a concave segment of the stress-stretch curve observed at small strains. Specifically, the stress reaches a peak, followed by softening. If fracture does not occur, the softening regime may be followed by a stiffening regime similar to the hyperelastic behavior of networks of high free volume. This is observed in dense nonwovens[26–28], in thermoplastics above the glass transition and some thermosets[29,30]. The behavior of a sparsely crosslinked thermoset may exhibit a concave segment, followed by softening and then stiffening, while the same material may be fully brittle when densely crosslinked. In this work we show that inter-fiber cohesion leads to the emergence of this type of behavior.

In the context of network materials, cohesion may be quantified using the elastocapillarity length[15,31], $L_{EC} = \sqrt{E_f I/\gamma}$, where E_f is the fiber material Young's modulus, I is the axial moment of inertia of the fiber cross-section ($I \sim d^4$ for circular cross-sections) and γ is the work of cohesion per unit length of contact between two parallel fibers. Cohesion has a significant effect on the mechanics of the network provided L_{EC} is smaller or equal to one of the length scales of the network, particularly the mean segment length, l_c, or d. Parameter L_{EC} was used to quantify the self-organization of carbon nanotubes in buckypaper and other fiber bundling processes[31]. For example, $L_{EC} = 10\ nm$ for single-walled CNT (10,10) of diameter 1.4 nm, while for microtubules $L_{EC} = 7$ to 20 μm[16].

While the mechanical behavior of networks without cohesion has been studied extensively, the effect of cohesion received much less attention. The self-organization of non-bonded fibers under the action of cohesive forces was discussed in Ref. 16 in terms of the non-dimensional parameter $\Psi = \left(L_0/L_{EC}\right)^2$, where L_0 is the fiber length. It was observed that the network self-organizes into a cellular network of fiber bundles provided $\Psi > a(\rho L_0)^2$, where a is a numerical parameter which depends on the friction between fibers[32]. Friction increases a, which then requires larger values of Ψ to drive network self-organization. The resulting cellular network has interesting, Ψ – dependent mechanical behavior, as discussed[33]. The mechanics of cross-linked networks with cohesion was studied using two-dimensional models[34]. It was observed that networks which are sub-isostatic in the absence of cohesion become isostatic and their stiffness increases as cohesion is enabled and then increased. It was also observed that the small strain behavior is primarily controlled by cohesion and less by the network structure. Despite the limitations of the work reported in Ref. 34 (2D models and only the small strain regime was investigated), the results indicate that exceptional behaviors, difficult or impossible to obtain without cohesion, can be achieved in such systems.

The present work reconsiders the effect of inter-fiber cohesion on the mechanical behavior of crosslinked networks by using 3D networks of fibers with various tortuosity and by using a

different modeling technology than in previous studies[34]. This allows reaching the large strain regime and imposes no limitations on the structure of the network used which, in turn, produces results with broader applicability. The central result reported is the emergence of a yield point as cohesion is enabled. However, since the present system is intrinsically elastic, the peak of the stress-strain curve is not a yield point (terminology implies association with plasticity) and as such, we refer to it as an 'unlocking phenomenon' with a corresponding unlocking stress, σ_u. The stress σ_u and the small strain stiffness increase as cohesion becomes stronger. It is shown that the response at strains beyond the unlocking point is controlled by the network and is largely unaffected by cohesion. The emergence of this unlocking phenomenon is a manifestation of the non-convexity of the energy surface over which the system with cohesion evolves.

2. Models and methods

2.1 Models

To generate the network models used in this study we start with periodic 3D Voronoi constructs. A cubic domain of edge length L is considered and a set of randomly distributed points, which act as seeds for the Voronoi procedure, are generated. Periodic images of the seed points are replicated in the 26 cubic domains of edge length L surrounding the reference cube. The entire $3L \times 3L \times 3L$ domain is then Voronoi tessellated and the edges of the resulting cells are taken as fibers, while the vertices represent crosslinks. Further, nodes are placed at each site where a fiber crosses the boundary of the central cube and only this reference domain is retained. This procedure produces a Voronoi structure which allows the application of periodic boundary conditions. This configuration of the network is here referred to as State 1, Fig. 1. We note that, since the present simulations are computationally expensive, working with the smallest possible models is highly desirable. However, as discussed in the literature[35–37], the mechanics of fiber networks is highly affected by size effects, which can be mitigated to some extent using periodic boundary conditions. This argument guided us towards considering a model that represents an infinite network structure which is periodic at length scales larger than L and stochastic at smaller length scales. This compromise is needed to render simulations tractable.

The fibers are modeled as Timoshenko beams and store energy in the axial, bending, torsion and shear modes[38]. As discussed in the literature, the bending mode dominates at relatively small strains, provided w is sufficiently small[1,39]. The beams cross-sections are considered circular, of diameter d. In any given model, all fibers are made from the same linear elastic material, of stiffness E_f, and have the same diameter, d. Parameter w, which controls the degree of non-affinity of the network behavior[1,39] is adjusted by varying d. The values of parameter w reported below refer to State 1 of the network.

The crosslinks are rigid, i.e. transmit both forces and moments, and the angle between fibers merging into a crosslink does not change during deformation. The connectivity number, which represents the number of fibers connected at each crosslink is $z = 4$. Based on the Maxwell criterion[40], three-dimensional structures of trusses (hinged crosslinks) with $z < 6$ are sub-isostatic and have vanishing stiffness. In this case, the network is stabilized by the bending mode of fibers and the type of crosslinks considered, and the small strain stiffness is non-zero. The pre-stress

introduced by the cohesion forces further stabilizes the structure[34]. Stabilization of sub-isostatic networks by pre-stress was also observed before in other contexts[41–43].

Cohesion between fibers is modeled by considering an attractive potential, u, which varies inversely with the distance R between two infinitesimal fiber segments. The resulting attractive force acting on a segment of infinitesimal length ds_1 interacting with a segment of length ds_2 located at a distance R is computed as $\mathbf{df} \sim ds_1 ds_2 \mathbf{R}/|\mathbf{R}|^3$, where $\mathbf{R}$ is the position vector of segment 2 relative to 1. The total force between two fiber segments of finite length is computed as a double integral of this expression along the two segments. The interaction is truncated at an outside cut-off radius $R_c^{out} = 1.03 l_{c0}$, where l_{c0} is the mean segment length of the Voronoi network in State 1, before cohesion forces are applied. This range was selected to ensure enough fiber segments in interaction with any reference fiber segment; note that the distribution of fiber lengths is Poisson, and hence a large number of fibers have length smaller than l_{c0}. The interaction is also truncated at an inner cut-off radius of $R_c^{in} = d$. Periodic boundary conditions are applied while computing cohesive interactions.

The strength of the interaction is controlled by the constant of proportionality in the $\mathbf{df} \sim ds_1 ds_2 \mathbf{R}/|\mathbf{R}|^3$ relation. However, as discussed in the Introduction, the relevant parameter of the problem is $\Psi = \gamma {l_{c0}}^2 / E_f I$. The work of cohesion, γ, is computed by considering two parallel and infinite fibers and computing the work per unit length required to separate the fibers from $R = R_c^{in}$ to $R = R_c^{out}$. The results are reported here in terms of Ψ.

This model implies that 'centers of interaction' are located along the centerline of each fiber and that two centerlines may only approach up to a distance d. This is adequate because the interaction forces considered are long ranged. If much shorter ranged interactions are considered, e.g. van der Waals, with the interaction force scaling as $1/R^n$, $n \gg 2$, it is necessary to consider that centers of interaction are uniformly distributed over the surface of cylindrical fibers and that the surface-to-surface interaction becomes important. Effective potentials for this situation have been developed[44], but are dependent on the local details of the geometry and are much more computationally expensive. It was determined that the 'large separation approximation' made in the present work is valid provided the wall-to-wall distance between fibers is larger than approximately $d/2$.[45] Since in the present case R_c^{out}/d ranges from 10 to 21 and hence much larger than 1, the large separation approximation is adequate. The case considered here, with $n = 2$ corresponds to Coulomb interactions between fibers due to distributed charge; cohesion due to dispersive interactions would require considering $n \gg 2$.

Contacts between fibers are allowed to form to ensure that fibers do not interpenetrate and cross during the simulation. The non-crossing condition is imposed by a constraint force proportional to the overlap of the fibers at the contact site acting in the direction normal to the contact (normal to the plane defined by the centerlines of the contacting fibers at the contact site). All contacts in the present models are frictionless.

Contacts also prevent the excessive collapse of the network under the action of cohesion forces. The distance between neighboring fibers is small in the vicinity of the crosslinks. To avoid

computational complexity and resolving unphysical interactions in the close vicinity of the crosslinks, we ignore cohesion forces acting within a distance of $1.5d$ from given crosslink along each fiber.

Two types of networks are considered which are referred to as type I and type II, respectively. A model of type I is generated by subjecting a Voronoi network to volume reduction corresponding to 20% reduction of the edge length of the initially cubic model in State 1. This is performed by directly simulating the hydrostatic compression of the State 1 Voronoi network without cohesion to the desired volume, followed by removing the stored strain energy. This defines a new configuration of the network, of edge length $L' = 0.8L$, in which fibers are crimped, but carry zero strain energy. This structure is then subjected to adhesive forces defined by the target Ψ parameter and the system is allowed to relax until a static equilibrium state is reached. The model volume in this state is somewhat smaller than L'^3, but the cohesion is not strong enough to produce excessive network collapse. This state of the network is referred to as State 2, Fig. 1. For example, for the network with $w = -3.94$ and the largest Ψ applied, $\Psi = 0.101$, the volume in State 2 is $V_0 = 0.953L'^3 = 0.488L^3$. No fiber-to-fiber contacts exist in State 1 and virtually no contacts form in State 2; the cohesive interactions are entirely balanced by the elasticity of the structure. State 2 is considered the reference state for the subsequent deformation of networks of type I.

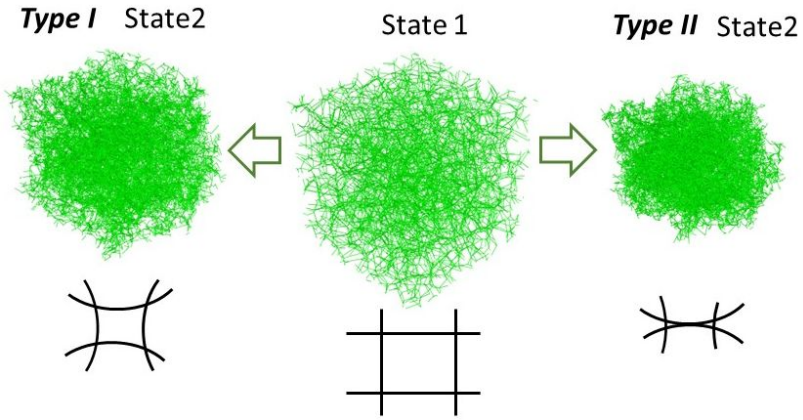

Figure 1. Representation of the network in the initial, Voronoi, State I, and in States II of the two types of structures considered. The schematics below the network images show the central concept behind the two types: cohesion deforms the fibers leading to some degree of structural collapse, which is smaller in type I compared to type II; contacts stabilize structures of type II, while only a small number of contacts are present in type I.

Type II networks are excessively collapsed. To generate such structures, large cohesive forces are applied to the initial Voronoi network in State 1 and the evolution of the model is simulated until equilibrium is reached and the kinetic energy is eliminated by damping (algorithmic friction with a fictitious background). These forces produce collapse of the structure and a large reduction of the unit cell volume. The structure is stabilized by inter-fiber contacts. Further, the strain energy of the resulting structure is eliminated and the large cohesion forces that produced the collapse are replaced with forces corresponding to the desired value of the Ψ parameter, followed by mechanical equilibration. Since the strain energy resulting from network collapse is removed, there

is no driving force for elastic rebound. Although some of the contacts formed during collapse are not engaged once the magnitude of the adhesive forces is modified, the resulting model is equilibrated primarily by contacts and less by the deformation of fibers. This is referred to as State 2 of the network of type II and is taken as reference for subsequent analysis of the mechanical response. The volume in State 2 is approximately $V_0 \approx 0.245L^3$, essentially independent of Ψ.

As a side product of model development, we investigated the critical pressure required to produce the collapse of Voronoi networks of various w parameters. This is discussed in the Supplementary information (SI). It is shown that the cohesive forces produce a hydrostatic stress state and the network collapses at a value of this stress which is identical to the pressure required to produce the same instability in the same network without cohesion. Further, this critical pressure scales as $p_c/E_f \sim \left(d/l_{c0}\right)^4$, which is reminiscent of the Euler buckling formula with an effective beam shape factor of 0.16 (see section 1 of SI for further discussion).

2.2 Implementation

Fibers are discretized using Timoshenko beam elements (B31 in Abaqus). The discretization is based on the contour length of the fibers. Specifically, fibers shorter than $l_{c0}/4$ are represented with a single element, while those longer than this threshold are discretized with up to 4 elements. This discretization was shown to lead to the optimal balance between accuracy (in both energy and network-scale stress) and computational cost[46].

For each element, the interaction force with all other elements within the cut-off radius of the potential, R_c^{out}, is computed analytically based on the current relative position of the fiber centerlines and approximating the elements to be straight line segments defined by their end nodes. The resulting force is applied as a distributed force along the respective element. Adhesive interactions also produce moments, which are computed analytically and applied as equivalent force dipoles on the respective element.

In the equilibration phase, the model is evolved until equilibrium is reached, while maintaining traction free boundaries. In the deformation phase, displacements are imposed in one direction (via controlling the size of the period unit cell in the respective direction) and traction free conditions are imposed in the two directions orthogonal to the loading direction. The cohesion forces are updated at every 2% global strain. Tests have been performed with various frequencies of cohesion force updating (from 0.1% to 3% strain) and it was concluded that the specified frequency leads to adequate results.

The solution is obtained using the commercial finite element software Abaqus/Explicit (version 62.5) under fully nonlinear conditions. Quasistatic loading conditions are ensured by using a sufficiently low value for the density of the fiber material to effectively eliminate the effect of inertia forces, using alpha damping, in which damping proportional to the velocity is applied, and keeping the total kinetic energy of the model below 5% of the total energy.

The stress reported here, σ, is the nominal stress evaluated based on the reaction forces computed at the moving boundary and the cross-sectional area of the model in the initial, unloaded State 2. The tangent stiffness, $E_t = d\sigma/d\lambda$, is computed based on the nominal stress. The Young's modulus of the fiber material, E_f, is used to normalize both stress and stiffness.

3. Results

Figure 2a shows nominal stress-stretch curves for networks of type I, with $w = -3.94$ and increasing values of the Ψ parameter. These networks are loaded in uniaxial tension starting from State 2. The network without cohesion, $\Psi = 0$, exhibit the hyperelastic behavior reported in the literature for structures of this type[1,23–25]. Specifically, an initial linear elastic regime can be identified, in which the small strain stiffness is constant, $E_t = E_0$, followed by a stiffening regime. These regimes are better visible in the tangent stiffness vs. stress representation of the data in Fig. 2a, shown in Fig. 3a. The stiffening regime is characterized by a slope of approximately 1, which corresponds to exponential stiffening. Most biological network materials[3–5], which are athermal, and fibrin gels[47], which are thermal, strain stiffen exponentially.

Cohesion has a significant effect on the stress-stretch curves. The small strain stiffness increases with increasing Ψ. Softening is observed immediately after the linear elastic regime and a maximum, which we refer to here as an unlocking phenomenon, emerges. As Ψ increases, the magnitude of the unlocking stress, σ_u, increases and the softening observed at larger strains becomes better defined. This is easily visible in Fig. 3a. Interestingly, the functional form of strain stiffening observed at even larger stretches is not affected by Ψ.

Figure 2b shows similar data for networks of type II, with $w = -3.94$, and with increasing values of the Ψ parameter, while Fig. 3b shows the corresponding tangent stiffness-stress data. The phenomenology observed in this case is similar to that reported for type I networks, although the stress and stiffness values are larger. Unlocking is observed in this case too, with σ_u increasing as Ψ increases.

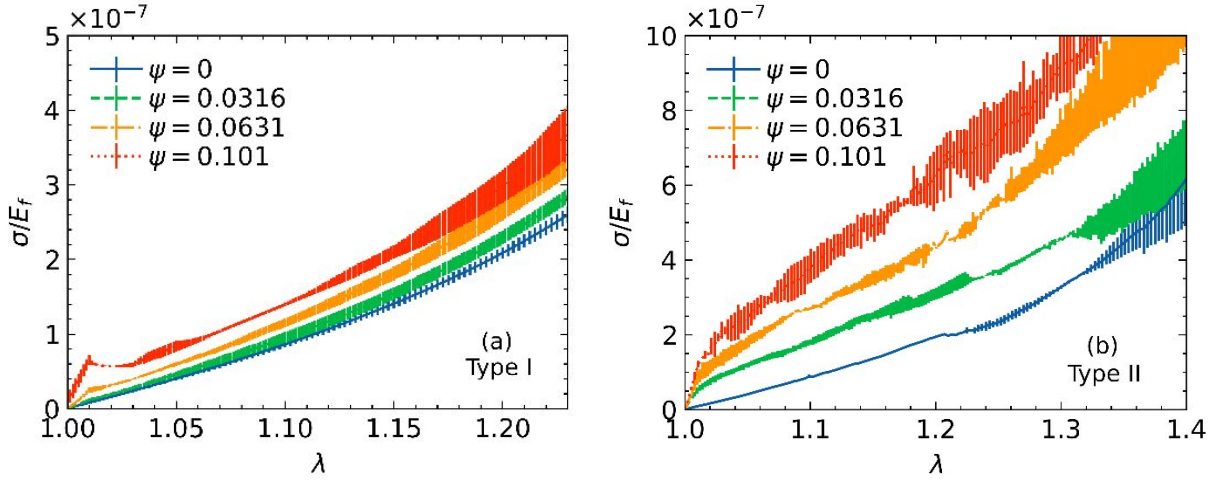

Figure 2. Nominal stress-stretch curves for (a) type I and (b) type II networks with $w = -3.94$, without cohesion ($\Psi = 0$) and with various levels of cohesion. The bars show the standard error computed with 3 realizations for each case.

A major difference between the two types of networks considered is related to the formation of contacts between fibers. The variation of the number of contacts during the deformation is shown in Fig. S2 of the SI for networks of types I and II and for $\Psi = 0$ and $\Psi = 0.101$. There are no contacts in State 2 for networks of type I and a negligible number of contacts form during loading. As discussed in section 2.1, this network preserves an open structure with large free volume and the cohesive forces are balanced by the elasticity of the structure. The opposite is true for the networks of type II. These are stabilized by the formation of many contacts in State 2. Since these are reminiscent of the network collapse procedure used to create the structure, contacts exist in the network without cohesion. Note that at $\lambda = 1$, in State 2, no contacts are activated/loaded when $\Psi = 0$. Some re-emerge immediately as λ increases above 1 and their number remains constant during the deformation, Fig. S2. Many contacts form when $\Psi > 0$ and these are loaded in State 2, when $\lambda = 0$, as well as throughout the deformation. Figure S2 indicates that their number remains approximately constant during deformation.

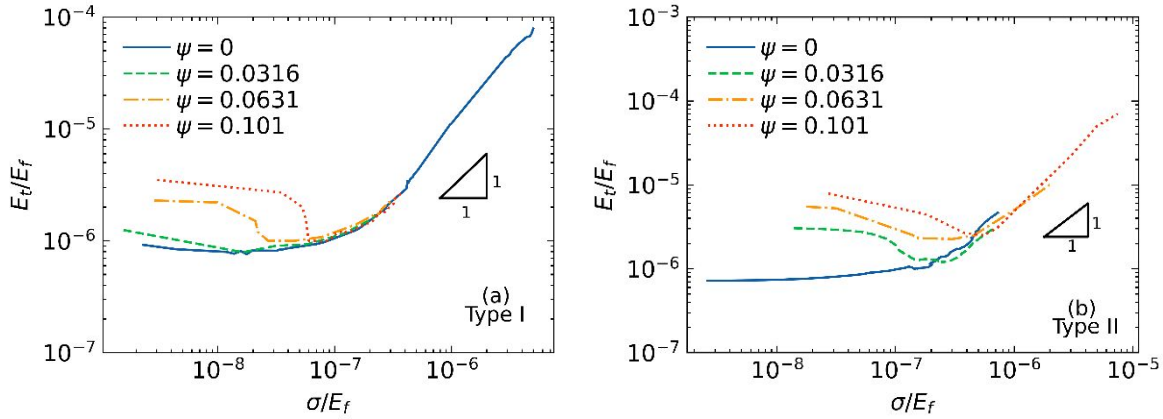

Figure 3. Tangent stiffness-stress curves for (a) type I and (b) type II networks with $w = -3.94$, without cohesion ($\Psi = 0$) and with various levels of cohesion corresponding to the curves in Fig. 1.

Interestingly, the presence of contacts does not change the functional form of strain stiffening. This is likely because the total number of contacts does not change significantly during the deformation. The strain at which stiffening becomes pronounced is larger in type II compared with type I networks, Fig. 2. This is attributed to the different crimp of the two types of networks in the unloaded State 2. The crimp parameter is computed here as the average of the ratio of the end-to-end length of fibers to the average contour length, and results $c_I = 0.957$ and $c_{II} = 0.847$ for State 2 networks of type I and II, respectively.

The above discussion indicates that the small strain response, including the unlocking point, are defined by the network structure and the cohesion. However, the large strain response is controlled by the network structure.

This behavior is observed in networks of different w. Figure 4 shows nominal stress-stretch curves obtained with models of type II and with $w = -3.28,\ -3.55,\ -3.94$. Several values of Ψ are considered for each w, with Ψ increasing as w increases (becomes smaller in absolute value) and the degree of non-affinity decreases. In all cases, the unlocking phenomenon emerges when $\Psi > 0$, while the softening response after unlocking becomes less pronounced at larger w due to the more rapid network-mediated strain stiffening.

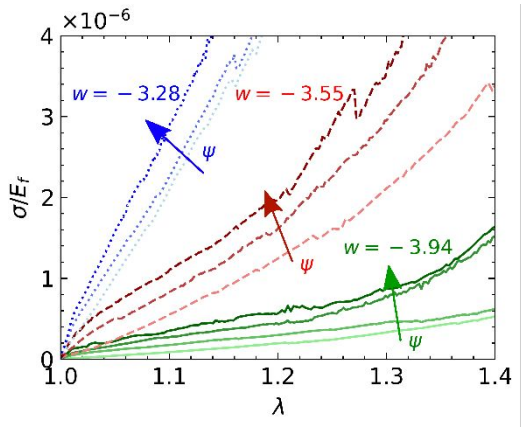

Figure 4. Stress-stretch curves for networks of type II of different w and Ψ values. Each group of curves corresponds to a w value, as indicated. Within each group, the curves move up as Ψ increases. The Ψ values considered for $w = -3.94$ are 0, 0.031, 0.063 and 0.101, for $w = -3.55$ are 0, 0.014 and 0.036, and for $w = -3.28$ are 0, 0.037 are 0.093.

It is of interest to determine the dependence of the small strain stiffness, E_0/E_f, and of σ_u/E_f, on w and Ψ. Based on the literature data, $E_0/E_f \sim \rho^2 d^4$ in the bending dominated, non-affine deformation regime of cellular networks without cohesion[48,49]. With $w = log_{10}\rho d^2$, it results that $E_0/E_f \sim 10^{2w}$. Figure 5a collects all data for networks of types I and II, all values of Ψ and w considered, and shows $E_0/f(w)E_f$ vs. Ψ, where $f(w) = 10^{2w}$. It is seen that data for various w collapses, which indicates that the w dependence of E_0 for Voronoi networks without cohesion in State 1, i.e. $f(w)$, applies to the present networks with crimp and with cohesion. The fact that the effect of crimp factors out from that of w in the definition of the small strain stiffness was also observed in networks without cohesion[50,51]. Hence, it results that a separable form such as:

$$E_0 \sim E_f f(w) g_E(\Psi) \qquad (1)$$

applies. The function $g_E(\Psi)$ is provided by the data in Fig. 5a and is approximated as linear, $g_E(\Psi) = a_E + b_E\Psi$. A linear fit leads to $a_E = 46.3$ and $b_E = 3435.4$ for type I and to $a_E = 66.2$ and $b_E = 8063.1$ for type II networks. In Ref. 34, the small strain stiffness of sub-isostatic 2D networks stabilized by cohesion was also seen to increase approximately linearly with Ψ. The stiffness of isostatic 2D networks was reported in the same reference to decrease with increasing cohesion, although the reference state was taken to be State 1 of the present discussion. In other works, it was reported that pre-stress leads to an increase of the network stiffness and this dependence is approximately linear[41,52].

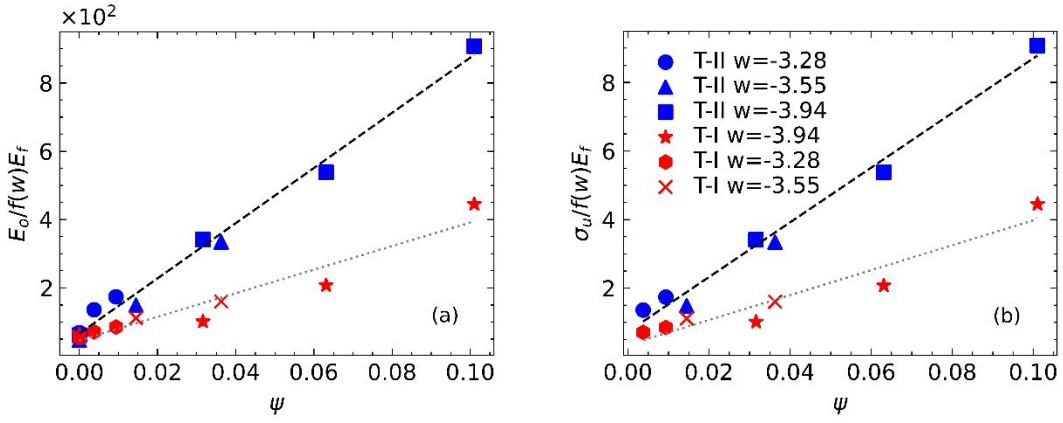

Figure 5. Variation of the normalized (a) small strain stiffness and (b) unlocking stress with Ψ for networks of types I and II (as T-I and T-II) and various w. The linear fits to the type I and type II data sets are shown.

Figure 5b shows the unlocking stress as a function of Ψ, for all w values considered. The vertical axis is normalized by $f(w) = 10^{2w}$, similar to Fig. 5a. The observations made in relation to E_0/E_f can be also made regarding σ_u/E_f: upon normalization of the vertical axis with $f(w)$, the data collapses, which indicates that $\sigma_u \sim E_f f(w) g_\sigma(\Psi)$. The function $f(w)$ is defined as $f(w) = 10^{2w}$, while $g_\sigma(\Psi)$ is defined by the data in Fig. 5b as being a linear function of Ψ, $g_\sigma(\Psi) = a_\sigma + b_\sigma \Psi$. A linear fit provides $a_\sigma = 0.351$ and $b_\sigma = 36.092$ for type I and to $a_\sigma = 0.735$ and $b_\sigma = 79.510$ for type II networks. Noting that the coefficient of Ψ is essentially identical in the two linear functions g_σ and g_E, i.e. $b_\sigma/a_\sigma \approx b_E/a_E$, it implies that the unlocking strain, ε_σ, is approximately identical in all these networks.

Increasing the crosslink density or/and the connectivity number, z, increases the small strain stiffness, E_0. While the effect of adhesive interactions is expected to remain qualitatively unchanged, it should become less prominent as E_0 increases. This is seen in Fig. 4 where unlocking becomes less visible as E_0 increases due to the increase of w, and at constant adhesion strength (constant Ψ).

To further clarify the nature of the unlocking, it is instructive to perform unloading and reloading. Figure 6a shows stress-stretch curves of a network of type I with $\Psi = 0.101$ subjected to continuous loading and to loading and unloading from two different maximum strains. Unlocking is observed during unloading as well, after which the system unloads in a linear elastic manner to (approximately) zero stress and strain. This is consistent with a modification of the energy surface caused by the cohesive interactions (emergence of local minima) which favors trapping in the current state. A hysteresis loop emerges, with the associated dissipation being caused by the multistability of the structure. Figure 6b shows a loading, unloading and reloading cycle overlapped to the continuous loading curve showing no history dependence of the loading path.

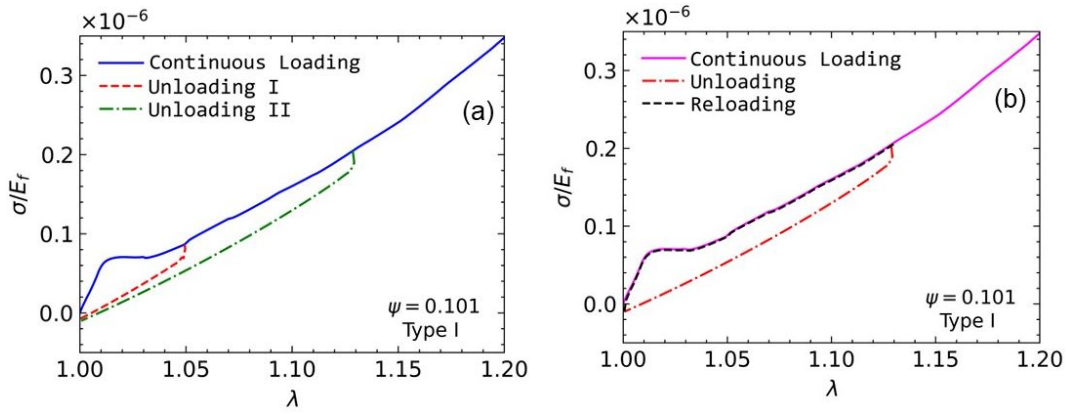

Figure 6. (a) Stress-stretch curves of a type I network subjected to continuous loading and to unloading from two levels of strain. (b) Stress-stretch curves of the same network subjected to loading, unloading and reloading.

An additional observation is that the cohesive forces produce a compressive hydrostatic system-level stress, $p(\Psi)$, which scales linearly with Ψ. The stress components are computed using the virial formula based on the cohesive pair interactions between elements (fiber segments) and are shown in Fig 7a for networks of type I with $w = -3.94$. The shear stress components are close to zero and the normal stress components are equal. The pressure is approximately constant as the network is stretched. The curves represent the average of three realizations. Figure 7b shows the associated variation of the volume for the same systems and loading history. The volume increases slightly with the applied strain and, for the range of strains considered, the variation is approximately linear. We note that the volume of a linear elastic continuum subjected to uniaxial deformation increases as $dV/V = (1-2\nu)\varepsilon$, where ν is the Poisson ratio of the respective material; the value of ν results weakly dependent of Ψ and equal to ~0.05 in this case. Furthermore, as discussed in the literature, volumetric increase is expected in networks of crimped fibers in the early stage of deformation[53], while large volume reduction is expected at later stages[25,50]. It results that cohesion works as an energy sink, such that part of the work performed is spent to increase the volume against the hydrostatic cohesion stress.

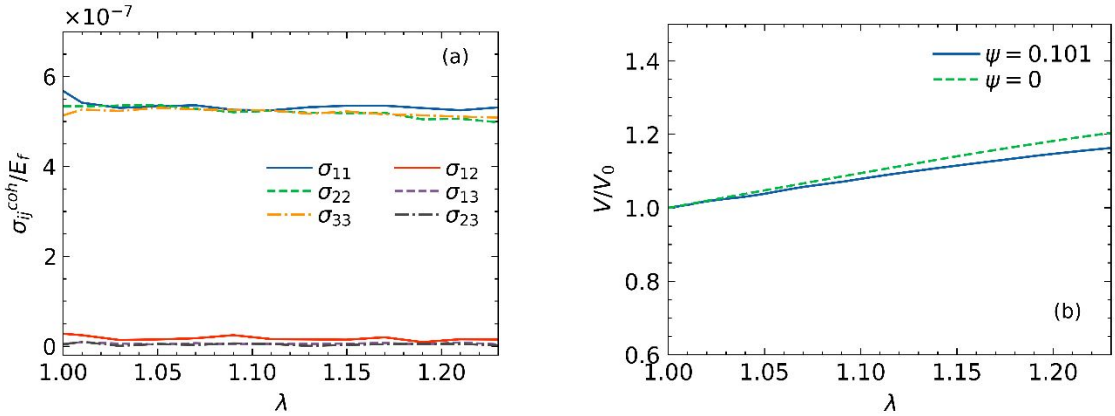

Figure 7. (a) Stress components produced by cohesion, σ_{ij}^{coh}, in type I networks with $w = -3.94$, and (b) variation of the volume in the same models and in the equivalent model without cohesion. Curves represent averages of three realizations.

In closure, it is necessary to place these observations, made using a model system, in relation with experimental observations of network behavior. The response of athermal network materials in uniaxial tension is of two general types: (i) purely hyperelastic behavior (convex stress-stretch curve), as observed in most collagen and elastin-based biological connective tissue[3–5,51], and (ii) a response that combines a concave segment (generically referred to as a yield point due to the visual similarity with the plastic yield point in metals) with a hyperelastic branch at larger strains (convex segment)[30,54]. Molecular networks also exhibit a yield point, which in elastomers is followed by softening[30,54,55]. If rupture does not occur, a stiffening branch is observed in elastomers at larger strains.

A concave stress-strain curve is typical for nonwovens[56,57] and networks of nanofibers (e.g. buckypaper[58]). On the other hand, network models, which generally do not account for inter-fiber interactions such as cohesion and friction, predict a purely hyperelastic response. Hence, it results that interactions between fibers taking place at sites other than the crosslinks may cause the concave stress-stretch segment. The present work demonstrates that adhesive interactions may produce this effect. We conjecture that, in the absence of cohesion, friction taking place at fiber-fiber contacts in crimped networks of low free volume may produce a similar phenomenon, which is expected to be the case in nonwovens. Since cohesion is short ranged, it is expected to play a minor role in networks composed of fibers of large diameter (e.g. > 1 μm), where friction may become the controlling mechanism. Cohesion is expected to be the dominant cause of the unlocking phenomenon in networks of nanofibers, both thermal (polymeric networks without solvent and above the glass transition temperature) and athermal (e.g. carbon nanotube, chitin, nanocellulose networks).

While the discussion above focuses on the emergence of the unlocking phenomenon in networks with elastic fibers, it is necessary to evaluate the likelihood for this behavior to be caused in realistic network materials by the yielding of elastic-plastic fibers[59]. This issue is discussed in Ref. 1, where it is shown that for non-affine networks composed from elastic-plastic fibers having yield strain ε_y^f, the network scale strain at which yield should be observed scales as $\varepsilon_y^f l_c/d$. This amplification of the network-scale yield strain relative to the fiber material yield strain by the segment aspect ratio, l_c/d, implies that fibers may not yield in low w networks with large l_c/d even at large strains. The physical origin of the amplification is related to the fact that thin fibers subjected to bending experience smaller maximum stress and strain as their diameter decreases and may remain in the elastic range even at large curvatures. This discussion implies that the unlocking phenomenon observed in network materials with low w is more likely to be caused by the mechanisms discussed in this article than by the onset of plastic deformation of fibers.

4. Conclusions

This work demonstrates the emergence of an unlocking phenomenon causing the stress-stretch curve of stochastic crosslinked networks to be concave at relatively small strains which is induced

by inter-fiber cohesion. These networks are isostatic and hyperelastic in the absence of cohesive forces. Cohesion leads to increased small strain stiffness and the emergence of an unlocking stress which increases as the cohesion strength increases. Softening follows unlocking, after which strain stiffening is observed. Cohesion has little effect on strain stiffening, which is controlled by the network architecture. The small strain stiffness and the unlocking stress may be expressed as the product of two functions of network parameters (w) and of the cohesion strength (Ψ), respectively. The present work also leads to the observation that a stochastic network subjected to compression due to hydrostatic boundary tractions or internal, inter-fiber attractive forces, loses stability at a critical pressure proportional to $\left(d/l_{c0}\right)^4$, which is a relation similar to the Euler buckling formula for single fibers subjected to axial compression. The study sheds light on the physical mechanism behind the unlocking (often referred to as a yield point) phenomenon observed in many network materials.

Acknowledgement

This research was supported by the National Science Foundation through grant CMMI- 2007909.

References

1 C. R. Picu, *Network Materials: Structure and Properties*, Cambridge University Press, Cambridge, 2022.

2 L. D. Black, P. G. Allen, S. M. Morris, P. J. Stone and B. Suki, *Biophys J*, 2008, **94**, 1916–1929.

3 S. J. Mostafavi Yazdi and J. Baqersad, *J Biomech*, 2022, **130**, 110864.

4 A. Mauri, A. E. Ehret, M. Perrini, C. Maake, N. Ochsenbein-Kölble, M. Ehrbar, M. L. Oyen and E. Mazza, *J Biomech*, 2015, **48**, 1606–1613.

5 L. W. Welling, M. T. Zupka and D. J. Welling, *Physiology*, 1995, **10**, 30–35.

6 R. Mao, S. Goutianos, W. Tu, N. Meng, G. Yang, L. A. Berglund and T. Peijs, *J Mater Sci*, 2017, **52**, 9508–9519.

7 K. Niskanen, Ed., *Mechanics of Paper Products*, Walter de Gruyter, Berlin/Boston, 2012.

8 K. B. Yilmaz, B. Sabuncuoglu, B. Yildirim and V. V Silberschmidt, *J Eng Fiber Fabr*, 2020, **15**, 1558925020970197.

9 H. S. Kim and B. Pourdeyhimi, *International Nonwovens Journal*, 2001, **os-10**, 1558925001OS–01000209.

10 S. S. Zumdahl, S. A. Zumdahl and D. J. DeCoste, *Chemistry*, Cengage Learning, United States, 11th edn., 2023.

11 A. G. Zilman and S. A. Safran, *Europhysics Letters (EPL)*, 2003, **63**, 139–145.

12 L. Onsager, *Ann N Y Acad Sci*, 1949, **51**, 627–659.

13 R. W. Style, A. Jagota, C.-Y. Hui and E. R. Dufresne, *Annu Rev Condens Matter Phys*, 2017, **8**, 99–118.

14 A. V. Linares, F. Vandevelde, J. Pantigny, A. Falcimaigne-Cordin and K. Haupt, *Adv Funct Mater*, 2009, **19**, 1299–1303.

15 M. De Volder and A. J. Hart, *Angewandte Chemie International Edition*, 2013, **52**, 2412–2425.

16 R. C. Picu and A. Sengab, *Soft Matter*, 2018, **14**, 2254–2266.

17 D. Wang, P. Song, C. Liu, W. Wu and S. Fan, *Nanotechnology*, 2008, **19**, 075609.

18 M. R. Islam and R. C. Picu, *J Appl Mech*, 2018, **85**, 85(8): 081011.

19 C. P. Broedersz and F. C. MacKintosh, *Rev Mod Phys*, 2014, **86**, 995–1036.

20 F. Burla, Y. Mulla, B. E. Vos, A. Aufderhorst-Roberts and G. H. Koenderink, *Nature Reviews Physics*, 2019, **1**, 249–263.

21 M. Alava and K. Niskanen, *Reports on Progress in Physics*, 2006, **69**, 669–723.

22 A. S. Shahsavari and R. C. Picu, *Philos Mag Lett*, 2013, **93**, 356–361.

23 A. Mauri, A. E. Ehret, M. Perrini, C. Maake, N. Ochsenbein-Kölble, M. Ehrbar, M. L. Oyen and E. Mazza, *J Biomech*, 2015, **48**, 1606–1613.

24 G. Žagar, P. R. Onck and E. Van Der Giessen, *Biophys J*, 2015, **108**, 1470–1479.

25 R. C. Picu, S. Deogekar and M. R. Islam, *J Biomech Eng*, 2018, **140**, 140(2): 021002.

26 D. Moyo, R. D. Anandjiwala and A. Patnaik, *Textile Research Journal*, 2016, **87**, 135–146.

27 M. Zhang, Y. Chen, F. Chiang, P. I. Gouma and L. Wang, *J Appl Mech*, 2019, **86**, 86(1): 011010.

28 L. Mezeix, C. Bouvet, J. Huez and D. Poquillon, *J Mater Sci*, 2009, **44**, 3652–3661.

29 Y. Qiao, L. D. Fring, M. R. Pallaka and K. L. Simmons, *Polym Compos*, 2023, **44**, 694–733.

30 L. R. G. Treloar, *Rubber Chemistry and Technology*, 1944, **17**, 813–825.

31 J. Bico, B. Roman, L. Moulin and A. Boudaoud, *Nature*, 2004, **432**, 690.

32 A. Sengab and R. C. Picu, *Phys Rev E*, 2018, **97**, 32506.

33 V. Negi and R. C. Picu, *Int J Solids Struct*, 2020, **190**, 119–128.

34 V. Negi and R. C. Picu, *J Mech Phys Solids*, 2019, **122**, 418–434.

35 A. S. Shahsavari and R. C. Picu, *Int J Solids Struct*, 2013, **50**, 3332–3338.

36 J. Merson and R. C. Picu, *Int J Solids Struct*, 2020, **206**, 314–321.

37 J. Dirrenberger, S. Forest and D. Jeulin, *Int J Solids Struct*, 2014, **51**, 359–376.

38 A. Öchsner, *Classical Beam Theories of Structural Mechanics*, Springer International Publishing, Switzerland, 2021.

39 D. A. Head, A. J. Levine and F. C. MacKintosh, *Phys Rev E*, 2003, **68**, 61907.

40 J. C. Maxwell, *The London, Edinburgh, and Dublin Philosophical Magazine and Journal of Science*, 1864, **27**, 294–299.

41 M. Sheinman, C. P. Broedersz and F. C. MacKintosh, *Phys Rev Lett*, 2012, **109**, 238101.

42 E. M. Huisman and T. C. Lubensky, *Phys Rev Lett*, 2011, **106**, 88301.

43 A. J. Licup, S. Münster, A. Sharma, M. Sheinman, L. M. Jawerth, B. Fabry, D. A. Weitz and F. C. MacKintosh, *Proceedings of the National Academy of Sciences*, 2015, **112**, 9573–9578.

44 M. J. Grill, W. A. Wall and C. Meier, *Int J Solids Struct*, 2023, **269**, 112175.

45 M. J. Grill, W. A. Wall and C. Meier, *Int J Numer Methods Eng*, 2020, **121**, 2285–2330.

46 N. Parvez, S. N. Amjad, M. Dey and R. C. Picu, *Fibers, 2023, submitted*.

47 S. B. Lindström, A. Kulachenko, L. M. Jawerth and D. A. Vader, *Soft Matter*, 2013, **9**, 7302–7313.

48 L. J. Gibson and M. F. Ashby, *Cellular Solids: Structure and Properties*, Cambridge University Press, Cambridge, 1997.

49 S. Deogekar and R. C. Picu, *J Mech Phys Solids*, 2018, **116**, 1–16.

50 A. Kabla and L. Mahadevan, *J R Soc Interface*, 2006, **4**, 99–106.

51 E. Ban, V. H. Barocas, M. S. Shephard and C. R. Picu, *J Appl Mech*, 2016, **83**, 83(4): 041008.

52 C. P. Broedersz and F. C. MacKintosh, *Soft Matter*, 2011, **7**, 3186–3191.

53 D. Rodney, B. Gadot, O. R. Martinez, S. R. du Roscoat and L. Orgéas, *Nat Mater*, 2016, **15**, 72–77.

54 Y. Kang, Z. Chen, Z. Jiao and W. Huang, *J Appl Polym Sci*, 2010, **116**, 1678–1685.

55 R. B. Dupaix and M. C. Boyce, *Polymer (Guildf)*, 2005, **46**, 4827–4838.

56 P. C. Patel and V. K. Kothari, *Indian J Fibre Text Res*, 2001, **26**, 409–413.

57 N. Chen, M. K. A. Koker, S. Uzun and M. N. Silberstein, *Int J Solids Struct*, 2016, **97–98**, 200–208.

58 S.-C. Her and W.-C. Hsu, *Nanomaterials*, 2020, **10**, 2258.

59 V. I. Räisänen, M. J. Alava, R. M. Nieminen and K. J. Niskanen, 1996, **11**, 243–248.